ACS SENSORS

Article

Cite This: ACS Sens. 2020, 5, 110−117

pubs.acs.org/acssensors

Fast and Reproducible ELISA Laser Platform for Ultrasensitive Protein Quantification

Xiaotian Tan,[†,⊥] Qiushu Chen,[†,⊥] Hongbo Zhu,[†] Song Zhu,[†,∥] Yuan Gong,[‡] Xiaoqin Wu,[†] Yu-Cheng Chen,[†,§] Xuzhou Li,[†] Maxwell Wei-Hao Li,[†] Wenyi Liu,[†] and Xudong Fan*[,†]

[†]Department of Biomedical Engineering, University of Michigan, 1101 Beal Avenue, Ann Arbor, Michigan 48109, United States

[‡]Key Laboratory of Optical Fiber Sensing and Communications, University of Electronic Science and Technology of China, No. 2006, Xiyuan Avenue, Chengdu 611731, P. R. China

[§]School of Electrical and Electronics Engineering, Nanyang Technological University, 50 Nanyang Avenue, 639798 Singapore, Singapore

[∥]Wuhan National Laboratory for Optoelectronics, Huazhong University of Science and Technology, Wuhan 430074, China

Supporting Information

ABSTRACT: Optofluidic lasers are currently of high interest for sensitive intracavity biochemical analysis. In comparison with conventional methods such as fluorescence and colorimetric detection, optofluidic lasers provide a method for amplifying small concentration differences in the gain medium, thus achieving high sensitivity. Here, we report the development of an on-chip ELISA (enzyme-linked immunosorbent assay) laser platform that is able to complete an assay in a short amount of time with small sample/reagent volumes, large dynamic range, and high sensitivity. The arrayed microscale reaction wells in the ELISA lasers can be microfabricated directly on dielectric mirrors, thus significantly improving the quality of the reaction wells and detection reproducibility. The details of the fabrication and characterization of those reaction wells on the mirror are described and the ELISA laser assay protocols are developed. Finally, we applied the ELISA laser to detecting IL-6, showing that a detection limit of about 0.1 pg/mL can be achieved in 1.5 h with 15 μL of sample/reagents per well. This work pushes the ELISA laser a step closer to solving problems in real-world biochemical analysis.

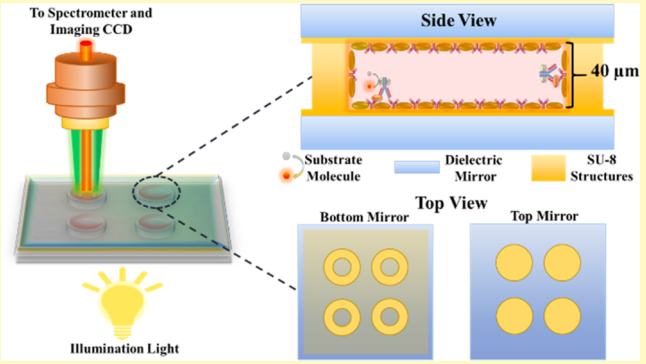

KEYWORDS: *optofluidic laser, microfabrication, Fabry−Perot cavity, ELISA, immunoassay, interleukin-6*

Enzyme-linked immunosorbent assay (ELISA) is one of the most popular methods used for the quantification of functional proteins in biological research and clinical diagnosis. Traditional ELISA is carried out in the wells of a microtiter plate (typically made from polystyrene).[1,2] However, the current sensing signal transduction mechanisms based on colorimetric,[2] fluorescence,[3,4] or chemiluminescence measurement[5,6] and the low surface-to-volume ratio (0.32 mm^{-1}) of reaction wells still limit the performance of ELISA, especially in terms of sensitivity (∼10 pg/mL), dynamic range (∼2−3 orders of magnitude), sample/reagent consumption (∼100 μL/well), and assay time (∼5 h).[6,7]

Optofluidic lasers as a new sensing transduction technique are being investigated for sensitive intracavity biochemical analysis such as DNA melting analysis,[8,9] sulfide ion sensing,[10] cellular analysis, and cancer diagnostics that are based on nucleic acid staining.[11−14] The intrinsic characteristics of the optofluidic laser enable optical amplification of small analyte concentration differences present in the gain medium, thus achieving a highly sensitive detection.[15,16] Additionally, the optical cavity acts as an optical filter to significantly reduce the fluorescence background for a high signal-to-noise ratio. Previously, the optofluidic laser based on a glass microfluidic capillary sandwiched between two gold-coated mirrors has been employed in ELISA to detect a type of cytokine and inflammatory marker IL-6 (Interleukin-6).[17] While a proof-of-concept optofluidic ELISA laser was demonstrated and high sensitivity was achieved, that optofluidic laser platform has a few drawbacks. First, due to the limitation in glass capillary fabrication, it is challenging to repetitively achieve nearly identical optical alignment conditions for the cavity, thus leading to batch-to-batch inconsistency in the cavity *Q*-factor among cavities, which ultimately causes low reproducibility and low reliability for ELISA laser measurement and limits the practical use of capillary-based ELISA laser systems. Moreover, since no surface modification was applied to the glass capillary

Received: September 15, 2019
Accepted: December 12, 2019
Published: December 12, 2019

DOI: 10.1021/acssensors.9b01795
ACS Sens. 2020, 5, 110−117

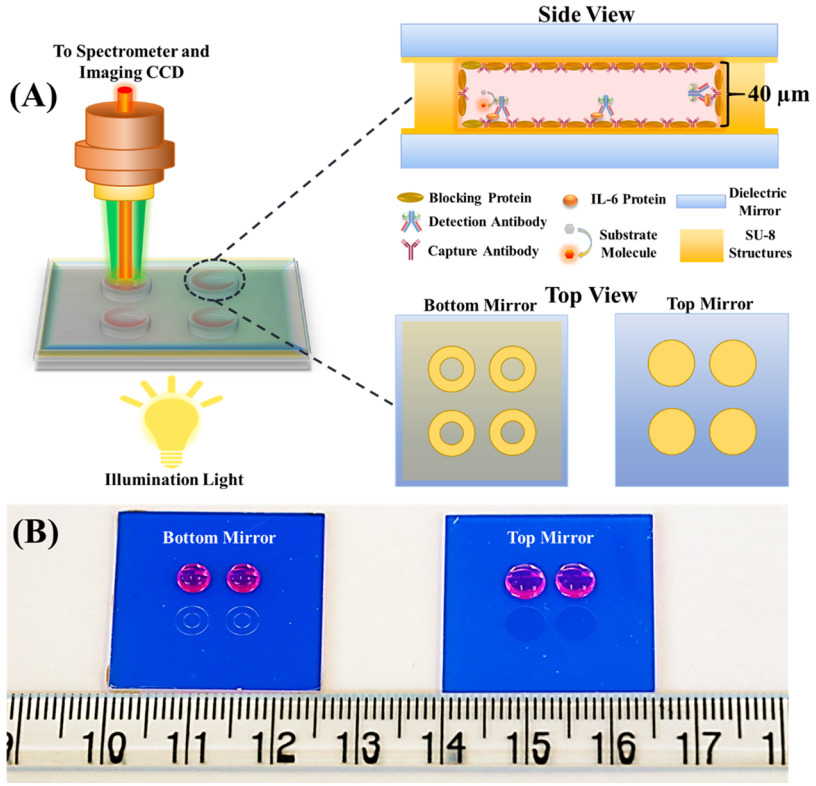

Figure 1. Layout, structures, and mechanism of the ELISA laser system. (A) Conceptual illustration of the ELISA laser experimental platform. The ELISA assay can be performed separately on the microfabricated bottom and top mirrors. Before taking measurements, the bottom and the top mirrors are sandwiched together and form a high-Q Fabry–Pérot (FP) cavity. (B) Photographs of the microfabricated bottom and top mirrors. The bottom mirror has four reaction wells, each of which had a diameter of 2 mm and a depth of ~42 μm. The top mirror also has four SU-8 flat pads that can be used for protein binding. They were fabricated at locations that can directly cover the wells on the bottom mirror. In each step of the immunoassay, 15 μL of reagents are added onto these designated wells and pads on both mirrors. The red droplets in the photograph indicate that liquid droplets can stably attach on the reaction sites during incubation.

ELISA reactors, the protein immobilization affinity was extremely low, resulting in a very long assay time (up to 7 h for laser measurements and up to ~8 h in total assay time).[6]

Here, we developed a novel, on-chip, optofluidic ELISA laser technique based on the Fabry–Pérot optofluidic laser platform. In this work, a chemically functionalized polymer substrate with a high protein affinity was directly microfabricated on dielectric mirrors that can be processed in batches with high reproducibility. The mirrors were divided into two groups, top mirrors and bottom mirrors, according to specially designed microscale reaction well structures on them. By sandwiching a top and a bottom mirror together, a microreactor with a high surface-to-volume ratio was formed in a well-spaced FP cavity. In this scheme, the repeatability and reliability of FP cavity mirror alignment and hence the ELISA laser measurement were drastically improved and the enzymatic fluorogenic reaction efficiency was significantly enhanced, resulting in a shortened assay time. With all these new designs, our ELISA laser technique is able to complete an assay within 1.5 h (including 30 min for laser measurement) while maintaining a small sample volume, large dynamic range (~4 orders of magnitude), and high sensitivity (LOD ~100 fg/mL for IL-6).

THEORETICAL ANALYSIS

The rate of the enzymatic reaction in a typical ELISA assay, v, can be described by the Michaelis–Menten equation[18]

$$v = \frac{\mathrm{d}[P]}{\mathrm{d}t} = k[\mathrm{E}]\frac{[\mathrm{S}]}{K_\mathrm{M} + [\mathrm{S}]} \quad (1)$$

where [P] is the enzymatic reaction product concentration, k is the enzymatic reaction rate, [E] is the enzyme concentration in an ELISA reactor, which is directly proportional to the quantity of immobilized analyte and detection antibody, [S] is the concentration of unreacted substrate molecule (as a function of time), and K_M is the Michaelis constant. Under our ELISA laser condition, the initial substrate concentration is orders of magnitude higher than K_M. During the initial stage of the reaction, the term $\frac{[\mathrm{S}]}{K_\mathrm{M} + [\mathrm{S}]}$ can be approximated as unity. As a result, the product concentration [P] increases over time, t, with a rate linearly proportional to the enzyme concentration, i.e.[17]

$$[\mathrm{P}] = k \times [\mathrm{E}] \times t \quad (2)$$

From a laser perspective, [P] represents the gain medium concentration in the ELISA laser. Initially, [P] is zero and no laser emission can be observed. However, [P] increases linearly with time based on eq 2 and the laser emission starts to emerge when the gain concentration reaches a threshold value, $[P]_{\mathrm{threshold}}$. Under fixed laser conditions with a given cavity Q-factor and given pump intensity, $[\mathrm{P}]_{\mathrm{threshold}}$ is a constant. The laser onset time, τ, is defined as the reaction time needed for an ELISA laser to reach $[\mathrm{P}]_{\mathrm{threshold}}$, i.e.,

DOI: 10.1021/acssensors.9b01795
ACS Sens. 2020, 5, 110–117

$$[\mathrm{E}]\cdot\tau = \frac{[\mathrm{P}]_{\mathrm{threshold}}}{k} = C \quad (3)$$

eq 3 shows that the laser onset time is inversely proportional to the enzyme concentration, and the overall reaction rate (defined as $1/\tau$) is directly proportional to the enzyme concentration. By measuring the laser-onset time, the enzyme concentration and hence the analyte concentration can be obtained.

MATERIALS AND METHODS

FP Cavity and Microwell Fabrication. FP cavities with integrated reaction wells were used to provide optical feedback for the ELISA laser. FP cavities were formed by sandwiching a top mirror and a bottom mirror. These mirrors were purchased from Evaporated Coatings Inc. (Willow Grove, PA). They were designed to have high reflectivity (99.5% according to the manufacturer's specifications) in the spectral range of 580−640 nm to provide the optimal optical feedback and a high transmission (>50%) in the spectral range of 520−540 nm to allow for external 532 nm laser excitation. The *Q*-factor of the FP cavity was on the order of 10^4 at a cavity length of 40 μm.

As illustrated in Figures 1A and S1A, the SU-8 reaction well structures for the ELISA laser experiment were fabricated on the mirrors by standard soft-lithography based on a method developed previously.[13] Two masks were used to fabricate the bottom piece with reaction wells and the top piece with flat pads, respectively. The mirrors were first plasma cleaned and dehydrated at 175 °C for 15 min. For the bottom piece, a 5 μm thick SU-8 2005 was first spin-coated on the mirror surface for better adhesion of successive SU-8 layers. This thin SU-8 adhesion layer was flood exposed and developed before a ∼42 μm thick SU-8 2010 layer was added on top. The mask containing microwells was used to expose the 42 μm SU-8 2010 layer (the height of the well is adjustable between 10 and 50 μm, depending on the fabrication protocols). After postexposure baking, the bottom mirror was developed and rinsed with isopropyl alcohol (IPA) and deionized (DI) water. The illustration for bottom mirror fabrication and the corresponding well structure can be found in Figure S1A,B. The wells such made had a diameter of 2 mm and a depth of ∼42 μm. The microfabricated bottom mirrors and wells have a high intra- and intermirror consistencies (see Figure S1C).

For the top mirror, a 5 μm SU-8 2005 layer was spin-coated on the substrate mirror, exposed with the mask containing the flat pad pattern, developed, and cleaned. Since the thermal conductivity of the glass-based substrate is lower than that of a standard silicon wafer, we found that elongated baking time and buffered cool down process would promote the adhesion of the SU-8 structure to the mirror. The photos of the microfabricated top and bottom mirrors can be found in Figure 1B. The microfabrication of both the top and bottom mirrors can be processed in batches, with high reproducibility. In the current work, up to 10 pieces of the top and bottom mirrors can be fabricated in each batch. Both the top and bottom mirrors can be reused after the ELISA laser reactions and measurements. The SU-8 structures can be removed with stainless steel blades. The mirrors were then sequentially rinsed with acetone, IPA, and DI water before starting the next round of SU-8 fabrication. The mirrors were reused up to 6 times without significant defects.

Top Mirror Silanization. SU-8 naturally has a medium-level affinity toward proteins.[19] To achieve optimal sensitivity (maximum protein affinity), we performed surface silanization to the microfabricated SU-8 structures on the top mirrors through the vapor phase deposition method.[20] The reagent used for surface silanization, 3-APTES ((3-aminopropyl)triethoxysilane), was purchased from Sigma-Aldrich (440140−100ML). As illustrated in Figure S2A, the silanization process has two steps: (1) treatment with air plasma for 30 s in a plasma etching machine for hydroxylation and (2) vapor phase 3-APTES deposition, which was carried out in a vacuum reactor with five drops of liquid 3-ATPES (∼100 μL) at 60 °C. The deposition process lasted for 3 h in a constant temperature oven. After the silanization treatment, both the SU-8 regions and the glass regions on the top mirror were coated with a layer of 3-ATPES, which has a primary amino group on one end of the chain. This amino group has a relatively high affinity for the free carboxyl groups found on aspartic acid, glutamic acid, and the C-terminus of proteins. The silanized top mirrors were ready to use after rinsing with DI water. Note that due to the relatively low chemical stability of SU-8 2010 used for reaction wells on the bottom mirror (i.e., SU-8 2010 structures will be damaged during the vapor phase 3-ATPES deposition at elevated temperature), the bottom mirror was not silanized. As presented in Figure S2B, the vapor phase silanization of the top mirrors can also be processed in batches with a metal steamer. Up to 10 pieces of the top mirrors can be simultaneously silanized in each batch.

Optical System Setup. A typical confocal microscopy setup was used to excite the sample and collect the emission light from the FP cavity. A schematic of our optical setup can be found in Figure S3. A pulsed optical parametric oscillator (OPO) laser (pulse width: 5 ns, repetition rate: 20 Hz) at 532 nm was used as the excitation source. In ELISA laser measurements, the pump intensity was fixed at approximately 210 μJ/mm^2. The emission light was collected through the same lens and sent to a spectrometer (Horiba iHR550, spectral resolution ∼0.2 nm) for analysis. An imaging CCD was used to facilitate focusing procedures and locate designated regions for laser examinations.

ELISA Reagents. The chemifluorescent substrate (QuantaRed Enhanced Chemifluorescent Horseradish peroxidase (HRP) Substrate Kit) was purchased from Thermo Fisher Scientific (15159). For IgG-HRP immobilization experiments, goat antimouse IgG (H + L) superclonal antibody with HRP conjugation was purchased from Thermo Fisher Scientific (A28177). For interleukin-6 (IL-6) ELISA laser experiments, human IL-6 DuoSet ELISA Kit (DY206), ELISA plate-coating buffer (1× phosphate-buffered saline (PBS), DY006), wash buffer (WA126), and reagent diluent (10% bovine serum albumin (BSA) in 10× PBS, DY995) were purchased from R&D Systems. The SuperBlock (PBS) Blocking Buffer (37515) and streptavidin poly-HRP (21140) was purchased from Thermo Fisher Scientific. Heat-deactivated human serum (H3667) was purchased from MilliporeSigma.

The stock solutions of the capture antibody, detection antibody, and human IL-6 standard were prepared according to the procedures described in the kits' user manuals. The working solution of wash buffer and reagent diluent were diluted with Milli-Q water (R = 18.2 Ω) to achieve 1× working concentration. The 1× reagent dilute solution (1% BSA in PBS) and SuperBlock Blocking Buffer were both used as the blocking buffers. The capture antibody stock solution was diluted with PBS buffer and finally achieved a concentration of 24 μg/mL (working concentration). The working solution of the biotinylated detection antibody was prepared by diluting the stock solution with the 1× reagent diluent and finally achieved an antibody concentration of 0.5 μg/mL (the detection antibody was biotinylated by the manufacturer). The concentrated human IL-6 standard was diluted to the desired concentration with the 1× reagent diluent. Streptavidin poly-HRP was employed to maximize the ELISA signal.[21] The working solution of streptavidin poly-HRP was produced by diluting the stock solution 1000 times in a customized dilution buffer (0.01% Tween 20 in 1% BSA).

IgG-HRP Binding Assay on Mirror. First, 15 μL of the HRP-conjugated IgG antibody solution (with various concentrations) was added to the designated reaction sites on the bottom and top mirrors (reaction wells on the bottom mirror and flat pads on the top mirror). IgG-HRP molecules contained in the solution were immobilized on the reaction sites through 90 min of incubation. Then, the reaction sites were rinsed with excessive amount of washing buffer. A few polystyrene beads 30 μm in diameter (purchased from Sigma-Aldrich (84135−5ML-F)) were placed into the reaction wells on the bottom mirror. Finally, 10 μL of QuantaRed fluorescent ELISA substrate solution was added into the reaction wells on the bottom mirror (no substrate was added to the pads on the top mirror). Then, the top mirror was placed upside down on top of the bottom mirror immediately so that the flat pads on the top mirror, which serve as

DOI: 10.1021/acssensors.9b01795
ACS Sens. 2020, 5, 110−117

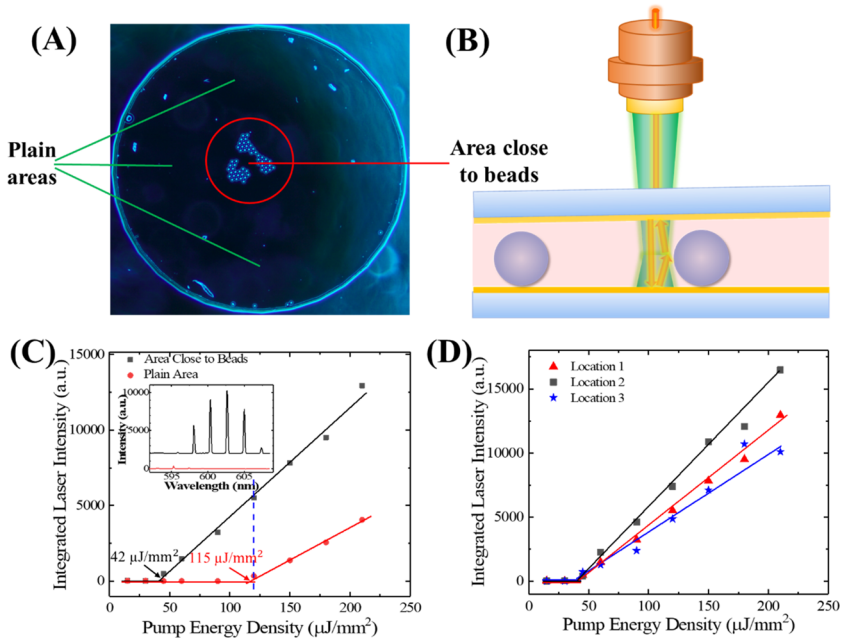

Figure 2. Demonstration of lateral optical confinement with polystyrene microbeads. (A) Photograph of polystyrene microbeads in a reaction well. The circled area indicates the location close to microbeads. (B) Illustration of the optical confinement and *Q*-factor improvement with a polystyrene bead. The light can be reflected by the boundaries of the beads, resulting in a lateral confinement of the optical mode, thus increasing the cavity *Q*-factor. (C) Laser characteristics comparison between the areas with beads and far away from the beads (plain area). The solid lines are the linear fit above the lasing thresholds. The lasing threshold was significantly reduced at the location close to beads (42 μJ/mm^2 versus 115 μJ/mm^2). (D) Lasing signals obtained at three different locations within the same well that were close to beads. Although the emission signals had different intensities, their thresholds were very close to each other (42 ± 3 μJ/mm^2).

caps of the ELISA reactors (see Figure S1D for illustration) cover the reaction wells on the bottom mirror. The sandwiched mirrors (along with the substrate solution between them) were then placed on the translation stage for measurement with the optical setup. An illustration of the structure of a pair of sandwiched mirrors can be found in Figure S1D.

IL-6 ELISA on the Mirrors. Before adding analyte (sample) solutions, capture antibodies were first immobilized on the designated reaction sites through 90 min of incubation. Then, the reaction sites on the top and bottom mirrors were both sequentially incubated with 1× reagent diluent and SuperBlock Blocking Buffer for 30 and 10 min. These steps were used to prevent nonspecific protein binding on the SU-8 structures. Then the analyte solution (with different IL-6 concentrations) was added to the reaction sites and incubated for 30 min. After that, the detection antibody solution was added to the reaction sites and incubated for another 20 min. Finally, the streptavidin poly-HRP solution was introduced to the reaction sites and incubated for an additional 10 min. At the beginning of all incubation steps, 15 μL of the solution was added to each of the reaction sites on both the bottom and top mirrors. To avoid contamination by residual reagents, at the end of all incubation steps, the remaining liquid on the mirrors was carefully and gently removed by placing water absorption tissues (KimWipes, Kimtech Science) on top of the reaction sites. Then, the mirrors were rinsed with excessive amount of washing buffer before a few polystyrene beads 30 μm in diameter were placed into the reaction wells on the bottom mirror. Finally, 10 μL of substrates solution was added into the reaction wells on the bottom mirror (no liquid was added to the flat pads on the top mirror). Then, the top mirror was placed upside down on top of the bottom mirror immediately. The sandwiched mirrors (along with the substrate solution between them) were then placed on the translation stage for measurement with the optical setup.

RESULTS

As presented in Figure 1A,B, in this work, microfabricated SU-8 reaction wells and flat pads were designed to perform solid-phase immunoassay and ELISA laser detection. A typical ELISA laser reactor setup contains two pieces of dielectric mirrors, one serving as the bottom mirror and the other as the top mirror. Four reaction sites were microfabricated in SU-8 on homologous locations on both mirrors. For the bottom mirror, the reaction sites were designed to have shallow well structures (approximately 42 μm in depth and 2 mm in diameter). In contrast, the reaction sites for the top mirror were simply SU-8 flat pads. When sandwiching the two mirrors together, a hollow reactor with a high surface-to-volume ratio (52 mm^{-1}) was formed between the aligned reaction sites.

Lateral Optical Confinement with Polystyrene Microbeads. We first investigated the optical characteristics of the FP ELISA laser cavity. As a noncrystal material, the borosilicate glass substrate that was used to fabricate dielectric mirrors has non-negligible elasticity under room temperature.[22] Due to the surface tension of water, when sandwiching the bottom and top mirrors together (with a proper amount of liquid in between), the intermirror distance at the center of the mirrors is slightly (~2−3 μm) shorter than the distance at the edges of the mirrors. In such a pair of mirrors, the resulting FP cavity with the highest *Q*-factor is typically located in the central region of the mirrors (between the four pairs of reaction sites). In other words, the region of the top mirror that directly covers the ELISA reaction wells is slightly tilted, leading to a deteriorated and not-well-controlled *Q*-factor. To achieve an acceptable *Q*-factor (approximately on the order of 10^4, see ref 23 for detailed calculations) for ELISA laser detection under nonperfect alignment conditions, polystyrene microbeads were added into the reactors, as illustrated in Figure 2A,B.[23] Due to the reflection effect at the boundary of a microbead, the lateral confinement in the lasing mode and significant improvement in the *Q*-factor can be achieved. This

DOI: 10.1021/acssensors.9b01795
ACS Sens. 2020, 5, 110−117

optical phenomenon is well explained in our recent publication.[23]

The performance of the bead-incorporated ELISA laser reactor was evaluated through a simple experiment. Before taking measurements, a few polystyrene microbeads ($d \approx 30$ μm) were placed in each reaction well on the bottom mirror. Then, 10 μL of the fully reacted (the enzymatic reaction reaches an equilibrium and the fluorescent molecule reaches maximum concentration) fluorescent substrate (4× recommended concentration) were added to the four wells on the bottom mirror. Then, a top mirror was placed on top of the bottom mirror with an upside down orientation (so, the SU-8 structures on both mirrors touched each other). The laser emission from locations that were close to or far away from beads were then collected. As shown in Figure 2C, the laser signal differs significantly between the areas close to beads and the areas far away from beads. The lasing threshold was significantly reduced, from 115 μJ/mm^2 at locations far away from any beads to approximately 42 μJ/mm^2 at locations close to the beads. In addition, as shown in Figure 2D, the lasing thresholds for the locations filled with beads are nearly identical, despite different lasing intensities. Therefore, the ELISA laser measurement can be carried out at any location filled with beads, which makes the experimental much easier and more consistent. For this reason, all of the data in the following experiments were collected from the regions that were filled with beads. Note that the total volume of the beads is typically smaller than 0.5% of a well's total volume (see Figure S4) and thus does not significantly alter the enzymatic reaction rate. Finally, Figure S5 shows the typical lasing spectrum, whose free spectral range is measured to be approximately 2.3 nm, which corresponds to a cavity length of approximately 55 μm, in good agreement with our laser cavity design (5 μm of SU-8 layers on both mirrors, 42 μm of ELISA microreactor, and 3 μm of water layer between the top and bottom mirrors).

Substrate Concentration Optimization. The concentration of fluorescent substrate (i.e., Thermo Fisher's QuantaRed) was optimized by monitoring the corresponding ELISA laser threshold. Since the absolute concentration of the substrate was not provided by the vendor, we used only the relative concentration. In this test, the substrate was prepared at 4×, 2×, 1× and 0.5× recommended concentrations. Higher substrate concentrations are not suitable for ELISA detection because of the strong nonspecific autoreaction. A 0.5 μL of high concentration free HRP was added into the substrates to artificially generate a saturated (fully reacted) condition before adding the HRP substrate samples into the reaction wells. The laser thresholds for these four concentrations were measured at regions close to microbeads inside the ELISA laser reactors. As shown in Figure 3, although laser signals are observed for all substrate concentrations, the lasing threshold for the 4× recommended substrate concentration appears to be the lowest and most reproducible. Furthermore, according to the 1× concentration result, we can conclude that the lasing can be observed with 4× substrate concentration when the reaction reaches 1/4 saturation. Therefore, the 4× recommended substrate concentration was selected as the experimental condition for all the following ELISA laser experiments, as it meets the requirements for low nonspecific autofluorescence (concentration not high), relatively easy generation of laser emission (low lasing threshold), and no need to wait for full saturation (1/4 saturation) when pumped at 210 μJ/mm^2.

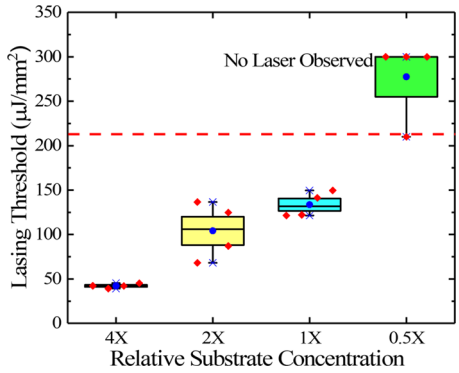

Figure 3. Lasing threshold for different substrate concentrations (fully reacted). All data were obtained at the locations close to the beads. The dashed red line represents the intensity, 210 μJ/mm^2, which was used as the pump for actual ELISA laser measurements. The red diamond dots represent the laser thresholds observed at different locations. For low substrate concentration (0.5×), almost no laser signal would be observed with the pump of 210 μJ/mm^2. For comparison, the lasing thresholds for the locations far away from any beads are given in Figure S6.

IgG-HRP Immobilization Experiments. To examine the stability of protein immobilization and the reliability for performing actual ELISA tests with this setup, we conducted a simplified protein immobilization test, which is the IgG-HRP immobilization experiment. In this set of experiments, HRP-conjugated IgG solutions (IgG-HRP dissolved in 1× PBS) with different concentrations were added into the microfabricated reaction wells on the bottom mirror and the flat pads on the top mirror. The detailed protocol can be found in "IgG-HRP binding assay on mirror" of the Materials and Methods section.

After 90 min of incubation, a portion of the IgG-HRP proteins was immobilized on the microfabricated SU-8 structures through hydrophobic interaction (physical adsorption). After adding QuantaRed ELISA substrate onto the wash buffer rinsed mirrors, the amount of immobilized IgG-HRP can be quantified through measuring the laser onset time (the reaction time used to generate the first laser emission). The time counting started immediately after sandwiching the top and bottom mirrors. Based on the reasons described in the previous subchapters, 210 μJ/mm^2 was selected to be the intensity of the pump laser and polystyrene microbeads were used to facilitate the generation of laser emission.

The result presented in Figure 4A shows the change in laser emission intensities over time for four different IgG-HRP concentrations over time. The intensities for each IgG-HRP concentration were presented with a time interval of 2 min, at a single location. As the result show, the laser signal emerges at different time points for different IgG-HRP concentrations. For IgG-HRP concentration at 10 μg/mL, the laser signal appears at the first minute (almost instantaneously) after adding substrate. For the other three IgG-HPR concentrations (1, 0.1, and 0.01 μg/mL), the laser signal first appears at 4, 8, and 20 min, respectively. As described in the theoretical analysis section, the difference in the laser onset time was caused by the difference in the quantity of HRP (as a subunit of the IgG-HRP molecule) that was immobilized on the mirrors. The wells with a higher amount of immobilized HRP will have a faster enzymatic reaction rate (positively correlation), thus requiring a shorter time to reach the

DOI: 10.1021/acssensors.9b01795
ACS Sens. 2020, 5, 110−117

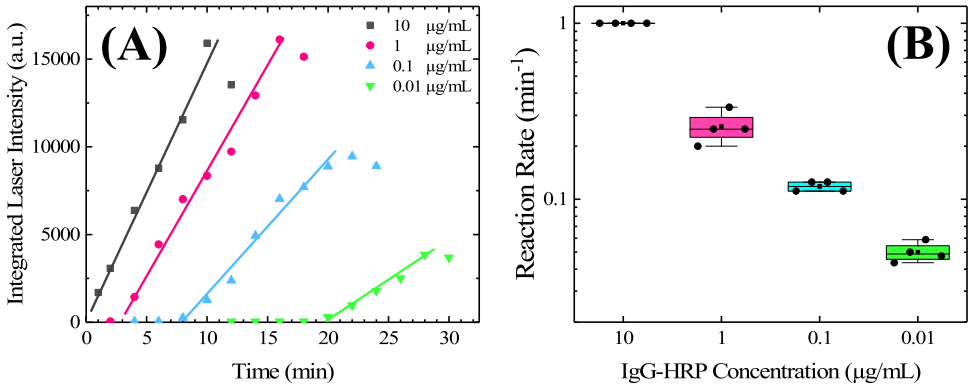

Figure 4. Results for IgG-HRP immobilization experiments. (A) Laser intensities vs time for four different IgG-HRP concentrations. The intensities are labeled as points with different colors. The solid lines are the linear about the threshold. An exemplary lasing spectra are given in Figure S7. (B) Reaction rates (defined as the inverse of the laser onset time) are measured for four different IgG-HRP concentrations. The black dots represent the reaction rate that were obtained from four different reaction wells on a set of mirrors.

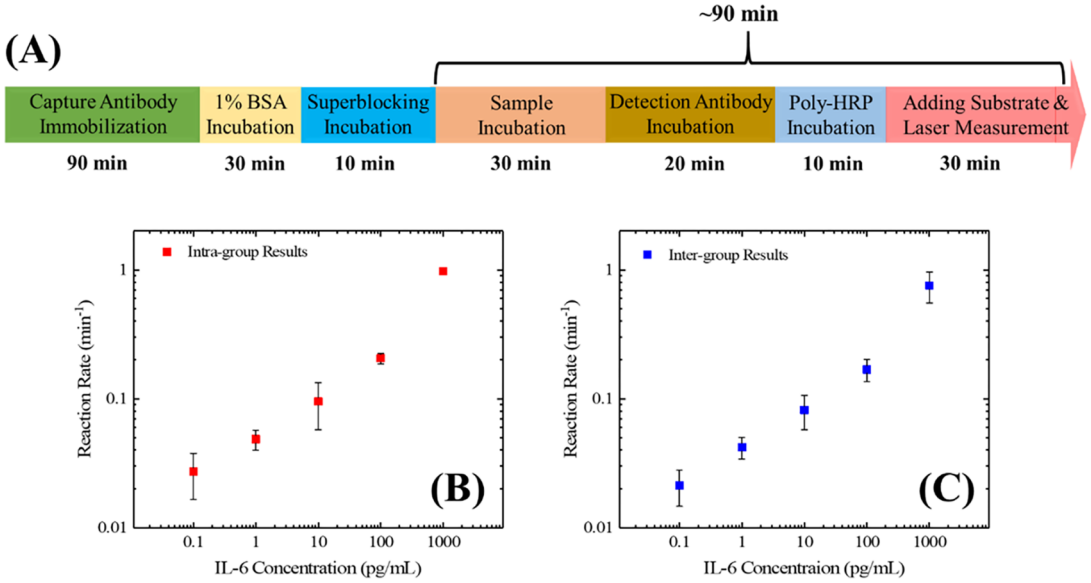

Figure 5. (A) Brief protocol for human IL-6 ELISA with our on-chip ELISA laser system. (B) Intragroup results for the IL-6 ELISA laser experiment. The reaction rate is defined as the inverse of the laser onset time. The error bars are the standard deviations measured with three reaction wells on the same set of mirrors. (C) Intergroup results for the IL-6 ELISA laser experiments. The data point on each concentration represent the overall averaged reaction rates that were measured from three sets of mirrors. The error bars are the standard deviations measured with three different sets of mirrors.

threshold fluorescent molecule concentration for laser emission. The corresponding overall reaction rate (defined as the inverse of the laser onset time, $1/\tau$) for all four IgG-HRP concentrations can be found in Figure 4B. This set of experiments clearly demonstrate that the ELISA laser is able to reliably distinguish IgG-HRP of different concentrations.

IL-6 ELISA Laser Experiments. The feasibility of performing real-world quantification of a specific protein with this setup was evaluated with a human IL-6 ELISA laser assay. Same as any other sandwich ELISA assay, the human IL-6 sandwich ELISA employs two antibodies that can recognize different epitopes on a single analyte (in our case, human IL-6) molecule. As illustrated in Figure 5A, in this experiment, the capture antibody was first immobilized (through physical adsorption) on the reaction sites on both the top and bottom mirrors. Then, after blocking with 1% BSA and SuperBlock Blocking Buffer, the solution containing analyte was added to and incubated with the mirrors. After the analyte was immobilized by the capture antibody, the biotinylated detection antibody solution and streptavidin poly-HRP solution was added and incubated with the reaction sites on the mirrors sequentially. One step of rinsing with 0.05% Tween-20 was performed between each of the incubation steps. By the end of the entire immunoassay, both the top and bottom mirrors were rinsed three times with ELISA wash buffer (0.05% Tween-20); then, tens of polystyrene microbeads (typically between 25 and 60 beads per well) were placed into the microreaction wells on the bottom mirrors (by dipping with dry pipet tips). Afterward, 10 μL of substrates solution (with 4× recommended concentration) was added into the reaction wells on the bottom mirror. Finally, the top mirror was placed on top of the bottom mirror with the substrate solution filling up all gaps in between. Then, the sandwiched ELISA laser cavity was taken to the optical setup for laser measurements. The total assay time was approx-

DOI: 10.1021/acssensors.9b01795
ACS Sens. 2020, 5, 110−117

imately 90 min, which was still considerably shorter than the traditional plate-based ELISA (about 6 h).[6]

In this experiment, the laser onset time in each reaction well was first recorded and then converted to reaction rates (inverse of the laser onset time). Figure 5B presents the intragroup results for five different IL-6 concentrations (0.1, 1, 10, 100, and 1000 pg/mL, respectively). The data were collected from the wells on one set of mirrors for each concentration. For all these five concentrations, the averaged reaction rate that was measured and calculated by subtracting the background reaction rate of 0.0246 min^{-1} from the background (i.e., 1% BSA in PBS serves as the blank sample, and the averaged laser onset time was 40.6 min). The intergroup measurements using multiple sets of mirrors are given in Figure 5C (three sets of mirrors for each concentration), showing that the sensing capability is reproducible across different sets of devices that were fabricated separately, which was significant improvement over our previous ELISA laser prototype.

To validate the ability of the ELISA laser to analyze complex samples, we also performed a set of experiments with IL-6 in human serum. The procedures were exactly the same as previously described, except that human serum was used. Figure 6 presents the results for six different IL-6

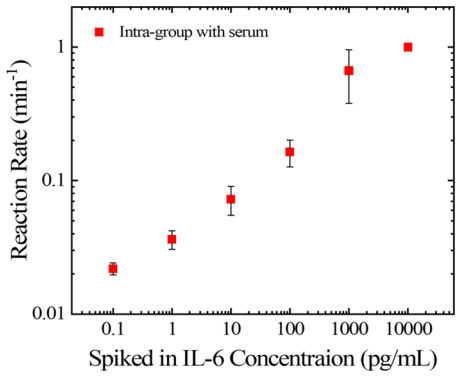

Figure 6. IL-6 ELISA laser results with human serum as analyte solvent. The error bars are the standard deviations measured with three reaction wells on the same set of mirrors. No laser was observed with the blank control.

concentrations that were spiked into human serum (0.1, 1, 10, 100, 1000, and 10 000 pg/mL, respectively). In this set of experiments, no laser was observed with the blank control (i.e., serum with no spiked IL-6) over the 60 min. Note that although the human serum usually contains ~0.5 to a few pg/mL of IL-6,[24,25] the background IL-6 did not show up in our measurement, which was further confirmed by a separate chemiluminescence-based ELISA showing that IL-6 in our serum sample was below 1 pg/mL. Therefore, no background reaction rate was subtracted in our data analysis. Similar to the results obtained with BSA buffer, the reaction rates for different concentrations generally follow a linear trend in the log−log scale between IL-6 concentration of 0.1 and 1000 pg/mL, which indicates our technique has a dynamic range of 4 orders of magnitude and a limit of detection (LOD) of 0.1 pg/mL. The IL-6 ELISA results shown above indicate while the ELISA laser technique still needs refinement, it has great potential to achieve high sensitivity (0.1 pg/mL) in a short amount of time (<1.5 h) with a small sample volume (30 μL) and a large dynamic range (4 orders of magnitude).

DISCUSSION AND CONCLUSIONS

In this work, we have successfully developed a new generation of ELISA laser platform able to carry out ultrasensitive quantification for specific proteins on a wide dynamic range in a short amount of time. This achievement is facilitated by the mass-production possibility of the microreaction wells on-chip, SU-8 microlithography technique, surface chemical modification, and lateral optical confinement. The new platform has significantly improved reproducibility over the previous ELISA laser prototypes and takes the ELISA laser a step closer toward real-world applications. Since sandwich ELISA itself is a widely used technology for analyte quantification, our technology should have similar or more potential application scenarios than other optofluidic immunoassays (e.g., turbidimetric immunoassays).[26] The microreaction wells also have the potential to be used as the reactors in liquid-phase laser-based biosensing experiments.[27] Our future work will include the integration of microfluidics and automated device for rapid and accuracy sample/reagent delivery and laser measurement. Clinically relevant biomarkers, such as IL-1β and IL-2 that require the detection of single-digital pg/mL to sub-pg/mL and that cannot be detected with regular ELISA techniques,[28,29] will also be explored.

ASSOCIATED CONTENT

Supporting Information

The Supporting Information is available free of charge at https://pubs.acs.org/doi/10.1021/acssensors.9b01795.

Photograph and illustration of the reaction well array on the bottom mirror (Figure S1); illustration of functionalization for the top mirror (Figure S2); schematic diagram of the optical setup (Figure S3); distribution of the polystyrene microbeads in the reaction wells (Figure S4); fluorescence and the laser spectra of QuantaRed substrate (Figure S5); lasing thresholds for different substrate concentrations (fully reacted) (Figure S6); example of the laser signal obtained at different time points in the IgG-HRP immobilization experiment (Figure S7) (PDF)

AUTHOR INFORMATION

Corresponding Author

*E-mail: xsfan@umich.edu.

ORCID

Yuan Gong: 0000-0001-6819-8402

Xudong Fan: 0000-0003-0149-1326

Author Contributions

⊥X.T. and Q.C. contributed equal to this work.

Notes

The authors declare no competing financial interest.

ACKNOWLEDGMENTS

The authors acknowledge the support from National Science Foundation under DBI-1451127 and ECCS-1607250.

REFERENCES

(1) Vanmechelen, E.; Vanderstichele, H.; Davidsson, P.; Van Kerschaver, E.; Van Der Perre, B.; Sjögren, M.; Andreasen, N.; Blennow, K. Quantification of tau phosphorylated at threonine 181 in human cerebrospinal fluid: a sandwich ELISA with a synthetic phosphopeptide for standardization. *Neurosci. Lett.* **2000**, *285*, 49−52.

DOI: 10.1021/acssensors.9b01795
ACS Sens. 2020, 5, 110−117

(2) O'Callaghan, J. P. Quantification of glial fibrillary acidic protein: comparison of slot-immunobinding assays with a novel sandwich ELISA. *Neurotoxicol. Teratol.* **1991**, *13*, 275−281.
(3) Konijn, A.; Levy, R.; Link, G.; Hershko, C. A rapid and sensitive ELISA for serum ferritin employing a fluorogenic substrate. *J. Immunol. Methods.* **1982**, *54*, 297−307.
(4) Noble, J. E.; Wang, L.; Cerasoli, E.; Knight, A. E.; Porter, R. A.; Gray, E.; Howe, C.; Hannes, E.; Corbisier, P.; Wang, J.; et al. An international comparability study to determine the sources of uncertainty associated with a non-competitive sandwich fluorescent ELISA. *Clin. Chem. Lab. Med.* **2008**, *46*, 1033−1045.
(5) Zhang, S.; Zhang, Z.; Shi, W.; Eremin, S. A.; Shen, J. Development of a chemiluminescent ELISA for determining chloramphenicol in chicken muscle. *J. Agric. Food Chem.* **2006**, *54*, 5718−5722.
(6) Tan, X.; Khaing Oo, M. K.; Gong, Y.; Li, Y.; Zhu, H.; Fan, X. Glass capillary based microfluidic ELISA for rapid diagnostics. *Analyst* **2017**, *142*, 2378−2385.
(7) Tan, X.; David, A.; Day, J.; Tang, H.; Dixon, E. R.; Zhu, H.; Chen, Y.-C.; Khaing Oo, M. K.; Shikanov, A.; Fan, X. Rapid Mouse Follicle Stimulating Hormone Quantification and Estrus Cycle Analysis Using an Automated Microfluidic Chemiluminescent ELISA System. *ACS Sens.* **2018**, *3*, 2327−2334.
(8) Hou, M.; Liang, X.; Zhang, T.; Qiu, C.; Chen, J.; Liu, S.; Wang, W.; Fan, X. DNA melting analysis with optofluidic lasers based on Fabry-Pérot microcavity. *ACS Sens.* **2018**, *3*, 1750−1755.
(9) Lee, W.; Chen, Q.; Fan, X.; Yoon, D. K. Digital DNA detection based on a compact optofluidic laser with ultra-low sample consumption. *Lab Chip* **2016**, *16*, 4770−4776.
(10) Gong, C.; Gong, Y.; Oo, M. K. K.; Wu, Y.; Rao, Y.; Tan, X.; Fan, X. Sensitive sulfide ion detection by optofluidic catalytic laser using horseradish peroxidase (HRP) enzyme. *Biosens. Bioelectron.* **2017**, *96*, 351−357.
(11) Chen, Y.-C.; Tan, X.; Sun, Q.; Chen, Q.; Wang, W.; Fan, X. Laser-emission imaging of nuclear biomarkers for high-contrast cancer screening and immunodiagnosis. *Nat. Biomed. Eng.* **2017**, *1*, 724.
(12) Chen, Y.-C.; Chen, Q.; Wu, X.; Tan, X.; Wang, J.; Fan, X. A robust tissue laser platform for analysis of formalin-fixed paraffin-embedded biopsies. *Lab Chip* **2018**, *18*, 1057−1065.
(13) Chen, Q.; Chen, Y.-C.; Zhang, Z.; Wu, B.; Coleman, R.; Fan, X. An integrated microwell array platform for cell lasing analysis. *Lab Chip* **2017**, *17*, 2814−2820.
(14) Chen, Y.-C.; Chen, Q.; Tan, X.; Chen, G.; Bergin, I.; Aslam, M. N.; Fan, X. Chromatin laser imaging reveals abnormal nuclear changes for early cancer detection. *Biomed. Opt. Express* **2019**, *10*, 838−854.
(15) Fan, X.; White, I. M.; Shopova, S. I.; Zhu, H.; Suter, J. D.; Sun, Y. Sensitive optical biosensors for unlabeled targets: A review. *Anal. Chim. Acta* **2008**, *620*, 8−26.
(16) Fan, X.; White, I. M. Optofluidic microsystems for chemical and biological analysis. *Nat. Photonics* **2011**, *5*, 591.
(17) Wu, X.; Khaing Oo, M. K.; Reddy, K.; Chen, Q.; Sun, Y.; Fan, X. Optofluidic laser for dual-mode sensitive biomolecular detection with a large dynamic range. *Nat. Commun.* **2014**, *5*, No. 4779.
(18) Cornish-Bowden, A.; Cornish-Bowden, A. *Fundamentals of Enzyme Kinetics*; Wiley-Blackwell: Weinheim, Germany, 2012; Vol. *510*.
(19) Blagoi, G.; Keller, S.; Johansson, A.; Boisen, A.; Dufva, M. Functionalization of SU-8 photoresist surfaces with IgG proteins. *Appl. Surf. Sci.* **2008**, *255*, 2896−2902.
(20) North, S. H.; Lock, E. H.; Cooper, C. J.; Franek, J. B.; Taitt, C. R.; Walton, S. G. Plasma-based surface modification of polystyrene microtiter plates for covalent immobilization of biomolecules. *ACS Appl. Mater. Interfaces* **2010**, *2*, 2884−2891.
(21) Ojeda, I.; Moreno-Guzmán, M.; González-Cortés, A.; Yáñez-Sedeño, P.; Pingarrón, J. Electrochemical magnetoimmunosensor for the ultrasensitive determination of interleukin-6 in saliva and urine using poly-HRP streptavidin conjugates as labels for signal amplification. *Anal. Bioanal. Chem.* **2014**, *406*, 6363−6371.
(22) Bansal, N. P.; Doremus, R. H. *Handbook of glass properties*; Elsevier, 2013.
(23) Wu, X.; Chen, Q.; Wang, Y.; Tan, X.; Fan, X. Stable high-Q bouncing ball modes inside a Fabry-Pérot cavity. *ACS Photonics* **2019**, *6*, 2470−2478.
(24) Sun, A.; Chia, J. S.; Chang, Y. F.; Chiang, C. P. Serum interleukin-6 level is a useful marker in evaluating therapeutic effects of levamisole and Chinese medicinal herbs on patients with oral lichen planus. *J. Oral Pathol. Med.* **2002**, *31*, 196−203.
(25) Fernández-Ruiz, M.; Humar, A.; Baluch, A.; Keshwani, S.; Husain, S.; Kumar, D. Baseline serum interleukin-6 to interleukin-2 ratio is associated with the response to seasonal trivalent influenza vaccine in solid organ transplant recipients. *Vaccine* **2015**, *33*, 7176−7182.
(26) Yang, X.; Shu, W.; Wang, Y.; Gong, Y.; Gong, C.; Chen, Q.; Tan, X.; Peng, G.-D.; Fan, X.; Rao, Y.-J. Turbidimetric inhibition immunoassay revisited to enhance its sensitivity via an optofluidic laser. *Biosens. Bioelectron.* **2019**, *131*, 60−66.
(27) Wu, J.; Fan, M.; Deng, G.; Gong, C.; Chen, K.; Luo, J.; Chiang, K. S.; Rao, Y.-J.; Gong, Y. Optofluidic laser explosive sensor with ultralow detection limit and large dynamic range using donor-acceptor-donor organic dye. *Sens. Actuators, B* **2019**, *298*, No. 126830.
(28) Di Iorio, A.; Ferrucci, L.; Sparvieri, E.; Cherubini, A.; Volpato, S.; Corsi, A.; Bonafè, M.; Franceschi, C.; Abate, G.; Paganelli, R. Serum IL-1β levels in health and disease: a population-based study.'The InCHIANTI study'. *Cytokine* **2003**, *22*, 198−205.
(29) Amado, I. F.; Berges, J.; Luther, R. J.; Mailhé, M.-P.; Garcia, S.; Bandeira, A.; Weaver, C.; Liston, A.; Freitas, A. A.IL-2 coordinates IL-2−producing and regulatory T cell interplay. *J. Exp. Med.* **2013**, *210*, 2707−2720.

DOI: 10.1021/acssensors.9b01795
ACS Sens. 2020, 5, 110−117